

The Gluon Propagator at High Temperature: Screening, Improvement and Non-Zero Momenta

U. M. Heller¹, F. Karsch² and J. Rank^{1,2}

¹ SCRI, Florida State University, Tallahassee, FL 32306-4130, USA

² Fakultät für Physik, Universität Bielefeld, P.O. Box 100131, D-33501 Bielefeld,
Germany

Abstract

We study the gluon propagator and the singlet potential in Landau gauge in the deconfined phase of SU(2) lattice gauge theory, using both the standard Wilson action and a tree-level Symanzik improved action. From the long-distance behavior of correlation functions of temporal and spatial components of the gauge fields we extract electric (m_e) and magnetic (m_m) screening masses. For the magnetic mass we find $m_m(T) = 0.456(6) g^2(T) T$. The electric mass can be described by a next-to leading order ansatz, obtained from one loop resummed perturbation theory. However, the best description is given by $m_e(T) = \sqrt{1.70(2)} g(T) T$. The electric screening mass thus is different from its lowest order perturbative prediction even for temperatures as high as $T \sim 10^4 T_c$.

1 Introduction

One of the main features of the high temperature plasma phase of QCD is the occurrence of chromo-electric and -magnetic screening masses (m_e and m_m) which control the infrared behavior of the theory [1]. The electric screening mass, which has been known in leading order perturbation theory for some time ($m_e \sim gT$), gives rise to the Debye screening of the heavy quark potential. The magnitude of m_e influences strongly the existence or non-existence of hadronic bound states in the high temperature phase. An understanding of its temperature dependence is therefore essential for any further analysis of the quasi-particle excitation spectrum in the QCD plasma phase. Also, a non-vanishing magnetic mass, which is entirely of non-perturbative origin and generally is expected to be $\mathcal{O}(g^2T)$, does contribute in next-to-leading order to m_e [2, 3]. Beyond leading order perturbation theory one thus needs a non-perturbative analysis also for the quantitative determination of the electric mass^a.

The definition of gluonic screening masses is not without problems. In general the masses are related to the low momentum behavior of the gluon propagator, $\Pi_{\mu\mu}(p_0, \vec{p})$. However, as the gluon propagator itself is a gauge dependent quantity it is not obvious that a “gluon mass” extracted from it would have a physical interpretation. Using the zero momentum limit ($|\vec{p}| \rightarrow 0$) in the static sector ($p_0 \equiv 0$) of $\Pi_{\mu\mu}$ does not yield a gauge invariant definition of the screening masses. It has, however, been shown [5, 6] that the pole masses defined through $m_\mu^2 = \Pi_{\mu\mu}(0, |\vec{p}|^2 = -m_\mu^2)$ are, within a wide class of gauges, gauge invariant to arbitrary order in perturbation theory. Exactly these pole masses are obtained from the exponential decay of finite temperature gluon correlation functions at large spatial separations. Although these correlation functions have to be calculated in a fixed gauge the pole masses extracted from them will be gauge independent. Alternatively one may insist on defining gluon screening masses through gauge invariant operators, e.g. Polyakov loop correlation functions, which are related to the heavy quark potential at finite temperature. Observables, which project onto states with the correct quantum numbers have been discussed in Ref. [7] and have recently been used to analyse the high

^aThe non-perturbative structure of the electric mass beyond leading order perturbation theory has recently also been discussed in [4]. The interesting possibility has been raised there that non-perturbative effects may arise even without generation of a non-vanishing magnetic mass.

temperature phase of QCD within the framework of dimensional reduction [8, 9]. In how far the definition of a screening mass through gauge invariant operators agrees with the pole mass has to be further analysed. The experience made with similar concepts in gauge-Higgs models shows that there is the possibility that gauge invariant operators only project onto a superposition of several elementary gluon excitations [10].

In this paper we analyse gauge dependent gluon correlation functions in Landau gauge. We have studied gluon correlation functions at finite temperature previously for the SU(2) gauge theory in a limited temperature interval ($1 < T/T_c < 20$) [11]. This analysis will be extended here in various ways. We have calculated magnetic and electric screening masses at much higher temperatures, up to $T \sim 10^4 T_c$, in order to analyse the approach to the perturbative regime. Furthermore, we study this time the dependence of the gluon correlation functions on momenta. In addition, we now also analyse the color singlet heavy quark potential, which at high temperatures is dominated by single gluon exchange. Moreover, we have also used a tree-level Symanzik improved gauge action in addition to the standard Wilson action in order to get some control over systematic lattice discretization errors.

In the next section we briefly discuss the observables we are going to analyse. In section 3 we define the actions we have used in our simulations and describe the procedure followed to fix the relation between bare gauge couplings and the temperature. The determination of electric and magnetic screening masses from gluon correlation functions is discussed in section 4. In section 5 we discuss the determination of the electric screening mass from the color singlet heavy quark potential. Furthermore we describe the influence of the improvement of the action on this potential. Finally, we give our conclusions in section 6.

2 Gluon Propagator on the Lattice

The main purpose of this investigation is an analysis of the gluon propagator at small momenta. We will extract screening masses from correlation functions of gauge fields $A_\mu(x_0, \vec{x})$ at large spatial separations. We will analyse dispersion relations for these screening masses in the static ($p_0 \equiv 0$) sector. For this purpose we introduce

momentum dependent gauge fields,

$$\tilde{A}_\mu(p_\perp, x_3) = \sum_{x_0, x_\perp} e^{i x_\perp p_\perp} A_\mu(x_0, x_\perp, x_3) \quad , \quad (2.1)$$

and the corresponding correlation functions

$$\tilde{G}_\mu(p_\perp, x_3) = \langle \text{Tr } \tilde{A}_\mu(p_\perp, x_3) \tilde{A}_\mu^\dagger(p_\perp, 0) \rangle \quad (2.2)$$

with $x_\perp = (x_1, x_2)$ and $p_\perp = (p_1, p_2)$. On a finite lattice, the momenta are given by $p_i = 2\pi k_i / (aN_i)$, with $k_i = -\frac{1}{2}N_i + 1, \dots, \frac{1}{2}N_i$ and N_i being the length of the lattice in the i -th direction.

The long-distance behavior of \tilde{G} yields the energy in the electric and magnetic sector respectively, i.e.^b

$$\begin{aligned} G_e(p_\perp, x_3) &\equiv \tilde{G}_0(p_\perp, x_3) \\ &\sim \exp\{-E_e(p_\perp) x_3\} \quad \text{for } x_3 \gg 1, \\ G_m(p_\perp, x_3) &\equiv \frac{1}{2} (\tilde{G}_1(p_\perp, x_3) + \tilde{G}_2(p_\perp, x_3)) \\ &\sim \exp\{-E_m(p_\perp) x_3\} \quad \text{for } x_3 \gg 1. \end{aligned} \quad (2.3)$$

For $p_\perp \equiv (0, 0)$ the long-distance behavior of these correlation functions thus defines electric and magnetic screening masses, which are related to the gluon polarization tensor,

$$m_\mu^2 = \Pi_{\mu\mu}(0, \vec{p}^2 = -m_\mu^2) \quad . \quad (2.4)$$

Using this definition, the leading correction to the lowest order perturbation theory result for the electric screening mass,

$$m_{e,0}(T) = \sqrt{\frac{2}{3}} g(T) T \quad , \quad (2.5)$$

^bNote that $\tilde{G}_3(p_\perp, x_3)$ is independent of x_3 in Landau gauge.

can be calculated in one-loop resummed perturbation theory. Based on the assumption that the infrared limit of the transverse gluon propagator is finite, $-\frac{1}{2}\Pi_{ii}(p_0 = 0, \vec{p} \rightarrow 0) = m_m^2 \sim g^4 T^2$, one obtains the gauge invariant result [2, 3]

$$m_e^2(T) = m_{e,0}^2 \left(1 + \frac{\sqrt{6}}{2\pi} g(T) \frac{m_e}{m_{e,0}} \left[\log \frac{2m_e}{m_m} - \frac{1}{2} \right] + \mathcal{O}(g^2) \right) . \quad (2.6)$$

As the magnetic mass appearing here is expected to be of $\mathcal{O}(g^2 T)$ the next-to-leading order correction is $\mathcal{O}(g \ln g)$.

It has been pointed out already sometime ago that the leading order perturbative calculation of the electric screening mass suffers from finite cut-off effects [12] similarly to what has been known for bulk thermodynamic observables, e.g. the Stefan-Boltzmann law for an ideal gas [13]. For the Wilson action the leading corrections are $\mathcal{O}((aT)^2)$, i.e. $\mathcal{O}(N_\tau^{-2})$. This is shown in Fig. 1. For large N_τ

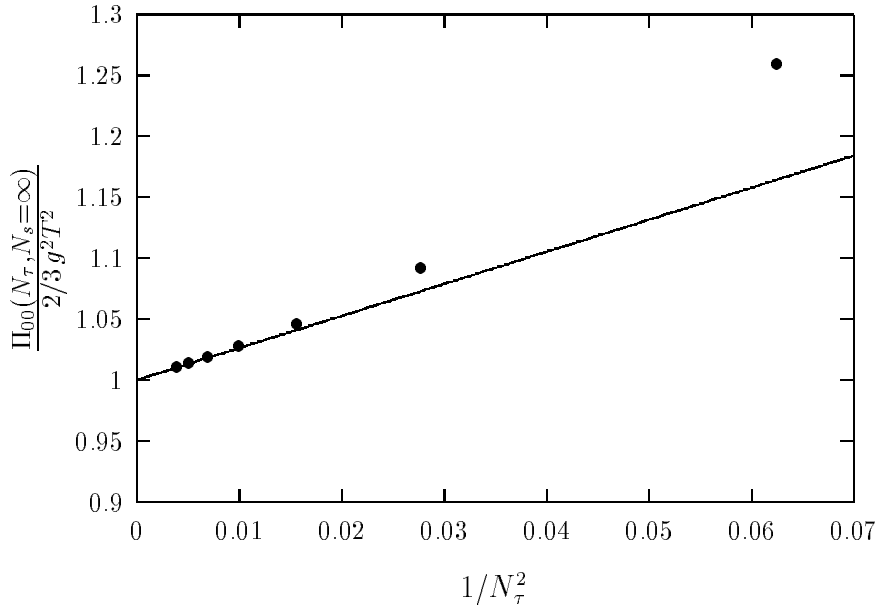


Figure 1: The polarization tensor Π_{00} at infinite N_s and various N_τ . The solid line shows the asymptotic result (2.7).

these deviations are due to the $\mathcal{O}(a^2)$ discretization errors introduced in the Wilson formulation. On a spatially infinite lattice we find for these cut-off errors

$$\frac{\Pi_{00}(N_\tau \rightarrow \infty, N_s = \infty)}{2/3 g^2 T^2} = 1 + N_\tau^{-2} \frac{1}{40\pi^2} \int_0^\infty dx x^5 \frac{\sinh x}{\sinh^4 \frac{x}{2}}$$

$$= 1 + \frac{4}{15} \left(\frac{\pi}{N_\tau} \right)^2, \quad (2.7)$$

which is similar in magnitude to the cut-off dependence of bulk thermodynamic observables like the energy density [14]. Using an improved action these leading cut-off errors are eliminated and corrections only start at $\mathcal{O}(N_\tau^{-4})$. In the case of the energy density or the pressure these actions lead to a strong reduction of cut-off effects in the high temperature limit [14]. In the following we will see, however, that this is not the case for the electric screening mass, i.e. the improvement of the ultra-violet sector does not influence the screening masses much.

3 Determination of the Temperature Scale

In our simulations we have used both the Wilson action (S_W) and a tree-level Symanzik improved action (S_I),

$$\begin{aligned} S_W &= \frac{\beta}{2} \sum_{1 \times 1} \text{Tr} U_{1 \times 1} \quad , \\ S_I &= \frac{\beta}{2} \left(\frac{5}{3} \sum_{1 \times 1} \text{Tr} U_{1 \times 1} - \frac{1}{12} \sum_{1 \times 2} \text{Tr} U_{1 \times 2} \right) \end{aligned} \quad (3.1)$$

where the sums run over all elementary 1×1 plaquettes $U_{1 \times 1}$ and planar 1×2 Wilson loops $U_{1 \times 2}$ ^c. The gauge dependent correlation functions have been calculated in Landau gauge, $|\partial_\mu A^\mu(x)|^2 = 0$. Details of our gauge fixing procedure are given in [11].

A comparison of simulations performed with these two actions on lattices with temporal extent $N_\tau = 4$ will allow to judge the cut-off dependence of our results. In the case of the Wilson action we also have performed calculations on lattices with temporal extent $N_\tau = 8$ in order to analyse the cut-off dependence for this action.

In order to quantify the influence of the non-zero cut-off at finite temperature one should, of course, compare calculations at the same physical temperature, $T \equiv 1/(N_\tau a)$. An accurate determination of the temperature scale also is needed for

^cIn the following, we will denote the couplings with β_W for the Wilson action and with β_I for the Symanzik improved action, respectively.

analyzing the dependence of the screening masses on a running coupling, $g(T)$. We thus start our analysis with the determination of temperature scales for both actions.

The problem to relate the temperature T to the coupling β is equivalent to the task of finding the dependence of the lattice spacing a on the bare coupling g^2 . We follow here the approach outlined in [15]. In order to take into account the violations of asymptotic scaling in the coupling regime of interest we use the general ansatz

$$a \Lambda_L = R(g^2) \cdot \lambda(g^2) \quad \text{with} \quad (3.2)$$

$$R(g^2) = \exp \left[-\frac{b_1}{2b_0^2} \ln(b_0 g^2) - \frac{1}{2b_0 g^2} \right] \quad , \quad (3.3)$$

$$b_0 = \frac{11N_c}{48\pi^2} \quad , \quad b_1 = \frac{34}{3} \left(\frac{N_c}{16\pi^2} \right)^2 \quad . \quad (3.4)$$

The function $\lambda(g^2)$ parameterizes the asymptotic scaling violations. For this we use an exponential ansatz

$$\lambda(g^2) = \exp \left[\frac{1}{2b_0^2} (d_1 g^2 + d_2 g^4 + d_3 g^6 + \dots) \right] \quad . \quad (3.5)$$

Using $T = 1/(N_\tau a)$ we obtain from Eq. (3.2)

$$\frac{1}{N_\tau R(g_c^2)} = \lambda(g_c^2) \frac{T_c}{\Lambda_L} \quad . \quad (3.6)$$

Here g_c^2 is the value of the bare coupling at the critical temperature T_c of the deconfinement phase transition at given N_τ . Using results for $g_c^2(N_\tau)$ [16, 17] the function $\lambda(g_c^2)$ is obtained from a fit where T_c/Λ_L is an additional free parameter.

Based on the Wilson action data for g_c^2 summarized in [16], the best fit in [15] is given by the parameterization $d_1 = d_2 = d_{n>3} = 0$. Their fit results are $d_3 = 5.529(63) \cdot 10^{-4}$ and $(T_c/\Lambda_L)_W = 21.45(14)$.

For the Symanzik improved action we have performed a similar fit, using the critical couplings computed in [17] for $N_\tau \geq 4$. Our best parameterization is given by $d_1 = d_{n>2} = 0$, and our fit results are $d_2 = 5.12(18) \cdot 10^{-4}$ and $(T_c/\Lambda_L)_I = 4.94(11)$. The fit can also be seen in Fig. 2.

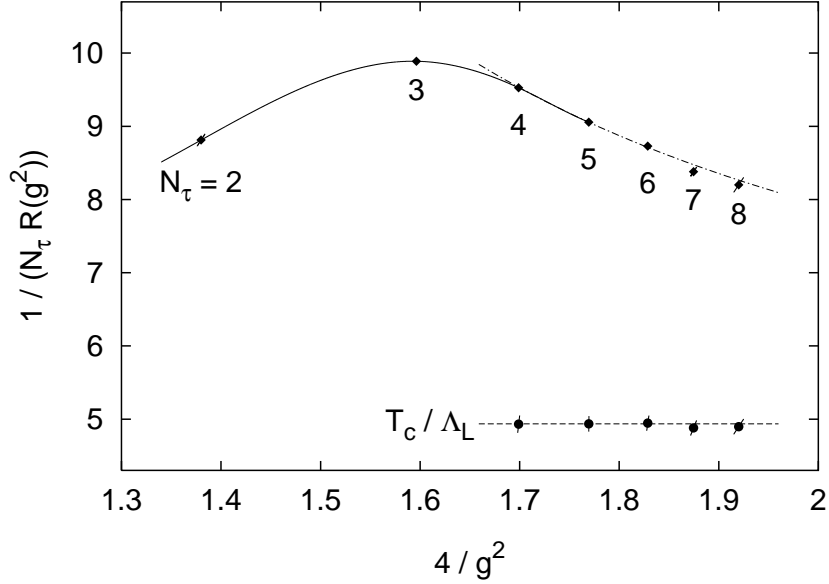


Figure 2: The critical temperature $1/(N_\tau R(g^2))$ vs. $4/g^2$ for $N_\tau = 2, \dots, 8$. The data for $g_c^{-2}(N_\tau)$ are taken from [17]. The solid line is a spline interpolation of the data, the dashed-dotted line is obtained from a fit for $N_\tau \geq 4$.

Using the perturbatively calculated ratios of Λ -parameter, i.e. $\Lambda_{L,I}/\Lambda_{L,W} = 4.13089(1)$ [18] and $\Lambda_{\overline{\text{MS}}}/\Lambda_{L,W} = 19.82314$ [19], we find for the critical temperature a result which, within 5%, coincides with the previously determined continuum extrapolation for the Wilson action

$$\frac{T_c}{\Lambda_{\overline{\text{MS}}}} = \begin{cases} 1.08 \pm 0.01 & \text{standard Wilson action [15]} \\ 1.03 \pm 0.03 & \text{tree level improved (1,2)-action} \end{cases} . \quad (3.7)$$

In the following, we will use an averaged value of $T_c/\Lambda_{\overline{\text{MS}}} = 1.06$.

We finally need to extract the temperature in units of the critical temperature at given N_τ . This is given by

$$\frac{T}{T_c} = \frac{R(g_c^2) \cdot \lambda(g_c^2)}{R(g^2) \cdot \lambda(g^2)} . \quad (3.8)$$

Using Eq. (3.8), the fit results for λ and the critical couplings from [16, 17] we can now relate the temperature T to the coupling $\beta = 4/g^2$. The results for the couplings used in our analysis are listed in Tab. 1. The good agreement found

$N_\tau = 4$		$N_\tau = 8$		$N_\tau = 4$	
β_W	T/T_c	β_W	T/T_c	β_I	T/T_c
2.512	2.004	2.74	2.007	1.92	1.984
2.643	3.002	2.88	3.031	2.063	3.031
2.74	4.013	2.97	3.929	2.152	3.923
2.88	6.062	3.12	6.016	2.30	5.979
2.955	7.527	3.20	7.530	2.382	7.528
3.023	9.143	3.27	9.151	2.452	9.149
3.219	15.88	3.47	15.89	2.652	15.88
3.743	66.78	4.00	66.71	3.183	66.68
4.24	253.5	4.50	253.3	3.684	253.2
4.738	953.1	5.00	953.9	4.185	954.0
5.238	3581	5.50	3578	4.685	3572
5.737	13383	6.00	13401	5.186	13393

Table 1: Relations between the couplings and the temperatures.

from this analysis for $T_c/\Lambda_{\overline{\text{MS}}}$ calculated with two different actions suggests that our temperature scale is of similar accuracy.

4 Screening Masses from Gluon Correlation Functions

In our earlier work [11] we have already investigated the behavior of the electric and magnetic screening masses in Landau gauge. Whereas in [11] we calculated the gluon propagator only at vanishing momentum, we now extend the analysis to finite momenta. Furthermore we are now using temperatures very much higher than in [11] in order to possibly get in closer contact with perturbation theory. Finally, we are now using in addition to the Wilson action also the tree-level Symanzik improved action.

In section 2 we have given the relations between the energies in the electric and magnetic sectors and gluonic correlation functions, Eq. (2.3). To extract the screening masses we use the dispersion relation between energy, screening mass and

momentum, which on the lattice has the form

$$\sinh^2 \frac{aE_i}{2} = \sinh^2 \frac{am_i}{2} + \kappa \sum_{j=1}^3 \sin^2 \frac{ap_j}{2} \quad , \quad i = e, m \quad . \quad (4.1)$$

In (4.1) we have introduced a factor κ which parameterizes deviations from a free particle dispersion relation ($\kappa \equiv 1$) introduced by a thermal medium.

Using $T = 1/(N_\tau a)$ we can now compute the screening masses in units of the temperature, m_i/T with $i = e, m$. We have performed simulations using the Wilson action on lattices of sizes $32^3 \times 4$ and $32^2 \times 64 \times 8$ and using the tree-level Symanzik improved action on a $32^3 \times 4$ lattice. At each value of the gauge coupling we performed measurements on at least 1000 configurations, see Tab. 2. Two consecutive

$32^3 \times 4$		$32^2 \times 64 \times 8$		$32^3 \times 4$	
β_W	meas.	β_W	meas.	β_I	meas.
2.512	2000	2.74	1220	1.92	2000
2.643	2000	2.88	1000	2.063	2000
2.74	2000	2.97	1000	2.152	2000
2.88	2000	3.12	1000	2.30	2000
2.955	2000	3.20	1000	2.382	2000
3.023	2000	3.27	1440	2.452	2000
3.219	2000	3.47	1140	2.652	2000
3.743	2000	4.00	1000	3.183	2000
4.24	2000	4.50	1160	3.684	2000
4.738	2000	5.00	1000	4.185	2000
5.238	2000	5.50	1000	4.685	2000
5.737	2000	6.00	1000	5.186	2000

Table 2: Number of measurement.

configurations were separated by at least 10 update iterations, and each update consists of at least four overrelaxation sweeps, followed by one heatbath sweep.

From the exponential decay of the gluon correlation functions G_e, G_m we extract the screening masses. A rather technical problem is the procedure to select a reliable

fit range in which $G_e(p_\perp, x_3)$ and $G_m(p_\perp, x_3)$ (see (2.3)) can be fitted to extract the energies in the electric and magnetic sectors. This is described in App. A.

The results for the screening masses (from the $\vec{p} = 0$ measurements) and the energies ($\vec{p} \neq 0$) are listed in Tabs. 3 and 4 respectively.

Wilson action, $32^2 \times 64 \times 8$ lattice					
β_W	$m_e(T)/T$	$m_m(T)/T$	β_W	$m_e(T)/T$	$m_m(T)/T$
2.74	2.39(11)	2.01(29)	3.47	1.62(4)	0.92(7)
2.88	1.95(4)	1.24(4)	4.00	1.62(8)	0.66(3)
2.97	1.91(7)	1.15(4)	4.50	1.55(5)	0.61(2)
3.12	1.92(9)	1.23(14)	5.00	1.41(3)	0.52(3)
3.20	1.92(10)	1.09(10)	5.50	1.27(5)	0.42(2)
3.27	1.93(6)	1.03(5)	6.00	1.26(5)	0.37(2)

Table 3: Electric and magnetic screening masses from $G_e(k_1 = 0)$ and $G_m(k_1 = 0)$.

4.1 Numerical Results for Zero Momentum

Let us first discuss the electric screening mass, extracted from the measurements at vanishing momentum $\vec{p} = 0$. In Fig. 3 we show m_e/T for both types of actions and the two different lattices we have used. One can see at once that, within errors, m_e/T does not differ significantly for the three sets. Even the tree-level Symanzik improved action, which cures discretization errors of $\mathcal{O}(a^2)$ in the action, does not shift the electric screening mass in any direction. This makes clear that ultra-violet modes do not contribute significantly to the screening mass. As a consequence, we have analysed all three data sets together.

Fig. 3 shows that m_e/T only depends very weakly on the temperature for small values of the coupling β , corresponding to temperatures less than about $10 T_c$. A constant fit in this temperature range yields $m_e(T)/T = 1.938(15)$. This behavior is qualitatively similar to what we have observed in [11]. For temperatures $1.3 T_c < T < 16 T_c$ we found in [11] $m_e(T)/T = 2.484(52)$. The difference between these values arises from different methods of extracting the screening masses. Whereas

Wilson action, $32^3 \times 4$ lattice			
β_W	$E_e(\vec{p}, T)/T$, extracted from		
	$G_e(k_1=0)$	$G_e(k_1=1)$	$G_e(k_1=2)$
2.512	2.14(11)	2.71(18)	2.46(5)
2.643	2.24(9)	2.28(8)	2.34(4)
2.74	1.94(5)	2.13(5)	2.33(7)
2.88	2.03(7)	2.03(4)	2.33(5)
2.955	1.87(4)	1.94(4)	2.27(5)
3.023	2.10(14)	2.12(13)	2.25(4)
3.219	1.80(7)	1.93(5)	2.03(3)
3.743	1.58(3)	1.78(7)	1.94(2)
4.24	1.64(8)	1.55(3)	2.01(4)
4.738	1.33(3)	1.51(4)	1.91(8)
5.238	1.19(2)	1.40(3)	1.83(4)
5.737	1.26(3)	1.35(4)	1.83(4)

Symanzik action, $32^3 \times 4$ lattice			
β_I	$E_e(\vec{p}, T)/T$, extracted from		
	$G_e(k_1=0)$	$G_e(k_1=1)$	$G_e(k_1=2)$
1.92	2.10(6)	2.18(5)	2.36(4)
2.063	1.96(5)	2.17(5)	2.36(4)
2.152	2.08(8)	2.04(5)	2.23(5)
2.30	1.76(3)	1.95(4)	2.91(26)
2.382	2.01(11)	2.00(4)	2.54(9)
2.452	1.70(5)	2.04(9)	2.21(5)
2.652	1.72(6)	1.53(21)	2.05(3)
3.183	1.69(8)	1.61(2)	2.13(11)
3.684	1.44(8)	1.75(6)	1.94(2)
4.185	1.50(6)	1.30(1)	1.85(4)
4.685	1.19(6)	1.45(7)	1.74(2)
5.186	1.31(8)	1.29(4)	1.77(5)

Table 4: Energies from the electric sector of gluon correlation functions.

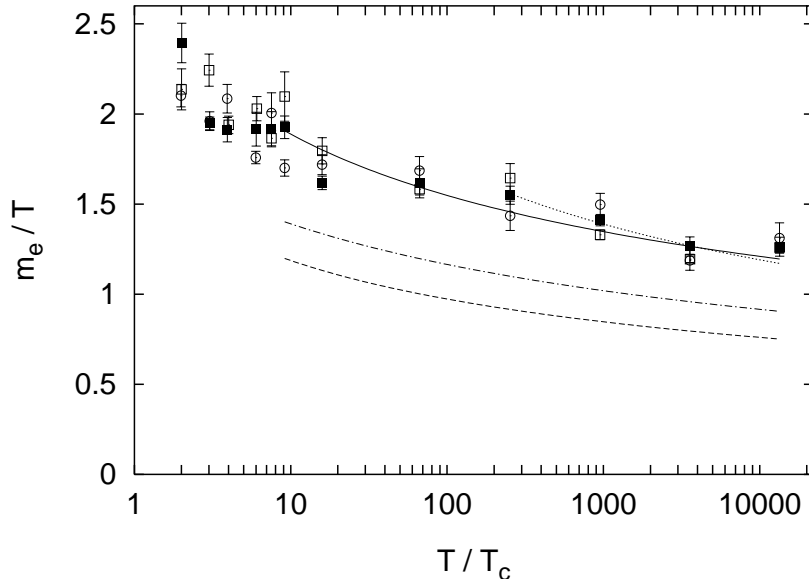


Figure 3: Electric screening masses in units of the temperature vs. T/T_c from simulations with Wilson action on $32^2 \times 64 \times 8$ (filled squares) and $32^3 \times 4$ (open squares) lattices and with Symanzik action on a $32^3 \times 4$ lattice (open circles). The dashed line is the tree-level result (2.5), the dashed-dotted line is a self consistent determination of m_e , using (2.6). The other lines are one parameter fits, using ansatz (4.4) (solid line, for $T \geq 9 T_c$) and ansatz (4.6) (dotted line, for $T \geq 250 T_c$) respectively.

in this paper we performed correlated fits of the gluon correlation functions over variable fit ranges (see App. A), we obtained m_e and m_m in [11] from uncorrelated fits in the fixed range $zT \geq 1$. Our new method results in screening masses which are up to 20% smaller. Since the method accounts for possible correlations in the data the results should be more reliable.

In contrast to [11] we have measured m_e now also at very high temperatures (up to $T \sim 13400 T_c$; see Tab. 1). From this analysis it becomes evident that m_e/T runs with T . Since this is expected from perturbation theory it is meaningful to test whether perturbative predictions also work quantitatively.

At lowest order perturbation theory for two color degrees of freedom and without taking dynamical quarks into account the electric mass is given by the well known relation (2.5). For the running coupling we use the 2-loop formula

$$g^{-2}(T) = \frac{11}{12\pi^2} \ln \frac{\mu}{\Lambda} + \frac{17}{44\pi^2} \ln \left[2 \ln \frac{\mu}{\Lambda} \right] \quad (4.2)$$

with $\mu = 2\pi T$ being the lowest lying Matsubara frequency. Hence

$$g^{-2}(T) = \frac{11}{12\pi^2} \left(\ln \frac{T}{T_c} + \ln \frac{2\pi T_c}{\Lambda} \right) + \frac{17}{44\pi^2} \ln \left[2 \left(\ln \frac{T}{T_c} + \ln \frac{2\pi T_c}{\Lambda} \right) \right] \quad . \quad (4.3)$$

We start the discussion of our data with a comparison with (2.5) which is shown in Fig. 3 as a dashed line. The numerical data for m_e are lying about 60% above the lowest order perturbative result (2.5). However, the functional dependence of the electric mass on the temperature seems to be well described by $m_e \sim gT$.

To verify the temperature dependence of the electric mass quantitatively we have performed several fits of m_e/T vs. $\ln(T/T_c)$ for temperatures $T \geq 9 T_c$. In our one parameter fits we fix the Λ -parameter appearing in the temperature dependent running coupling to $\Lambda_{\overline{\text{MS}}}$ and therefore use the MC-result for $T_c/\Lambda_{\overline{\text{MS}}}$, i.e. $T_c/\Lambda_{\overline{\text{MS}}} = 1.06$. In those cases where we parameterize the screening masses only by its leading g^2 dependence the effect of higher order corrections can be partially taken into account in a modification of the Λ -parameter. We, therefore, also performed two parameter fits with a free ratio $\Lambda_{\text{fit}}/\Lambda_{\overline{\text{MS}}}$.

The first fit ansatz we use is

$$\left(\frac{m_e(T)}{T} \right)^2 = A_{\text{fit}} g^2(T) \quad . \quad (4.4)$$

The results obtained with this ansatz are summarized in Tab. 5. They again reflect

1-parameter fit		2-parameter fit	
A_{fit}	1.69(2)	A_{fit}	1.92(9)
$\Lambda_{\text{fit}}/\Lambda_{\overline{\text{MS}}}$	1	$\Lambda_{\text{fit}}/\Lambda_{\overline{\text{MS}}}$	0.33(13)
χ^2/dof	4.51	χ^2/dof	4.14

Table 5: Fit results of $(m_e(T)/T)^2$, extracted from gluon correlation functions at zero momentum, using the fit ansatz (4.4).

that the lowest order perturbative result (2.5) does not describe the data very well. The fit parameter A_{fit} is much too big compared to its theoretical value 2/3. The solid line shown in Fig. 3 is the result from the one parameter fit. It shows, as noted above, that at least the variation of m_e/T with the temperature is well described by

ansatz (4.4). However, the temperatures we have used are apparently still too low to get in contact with lowest order perturbation theory.

To test the next-to-leading order result (2.6) we also determined the ratio m_e/m_m and especially the magnetic mass. We were only able to extract a reliable result for m_m for the lattice with spatial extension $N_3 = 64$. On the smaller lattice the local screening masses $m_m(x_3, T)$ do not reach a plateau (see App. A). Therefore the fits of the correlation function G_m were quite poor, i.e. had a large χ^2 . As the electric screening masses obtained from different actions and lattice sizes do not show any significant difference, we expect that also the magnetic mass does not show a significant ultra-violet cut-off dependence.

In Fig. 4a we show the electric and magnetic screening masses, obtained from the Wilson action simulation on the $32^2 \times 64 \times 8$ lattice. Fig. 4b gives the squared ratio $(m_e/m_m)^2$. Our data strongly suggest a temperature dependence of the form $(m_e/m_m)^2 \sim g^{-2}(T)$, which is in agreement with the general expectation $m_m(T) \sim g^2(T) T$. We therefore performed a fit according to

$$\left(\frac{m_e(T)}{m_m(T)}\right)^2 = C_{\text{fit}} g^{-2}(T) \quad . \quad (4.5)$$

A two parameter fit in the range $T \geq 2 T_c$ yields $C_{\text{fit}} = 9.16(69)$, $\Lambda_{\text{fit}}/\Lambda_{\overline{\text{MS}}} = 2.42(64)$ with $\chi^2/\text{dof} = 0.79$. Fixing the Λ -parameter to $\Lambda_{\overline{\text{MS}}}$, a one parameter fit results in $C_{\text{fit}} = 7.46(27)$ and $\chi^2/\text{dof} = 1.35$. In Fig. 4b we have shown the two parameter fit.

With these results in hand we are now able to check the next-to leading order result for m_e . The dashed-dotted line in Fig. 3 is a selfconsistent determination of m_e , using (2.6). It lies about 20% above the lowest order prediction and therefore is closer to our data. However, it is still too low to describe the data well. Therefore we have performed additional fits of the electric mass that take into account higher order corrections. Based on (2.6) we use the ansatz

$$\left(\frac{m_e(T)}{T}\right)^2 = \frac{2}{3} g^2(T) \left(1 + \frac{\sqrt{6}}{2\pi} g(T) \left[\log \frac{2m_e}{m_m} - \frac{1}{2}\right]\right) + B_{\text{fit}} g^4(T) \quad . \quad (4.6)$$

As the g^4 correction term leads to a temperature dependence which is too strong within the entire T -interval, we have restricted the fit to very high temperatures,

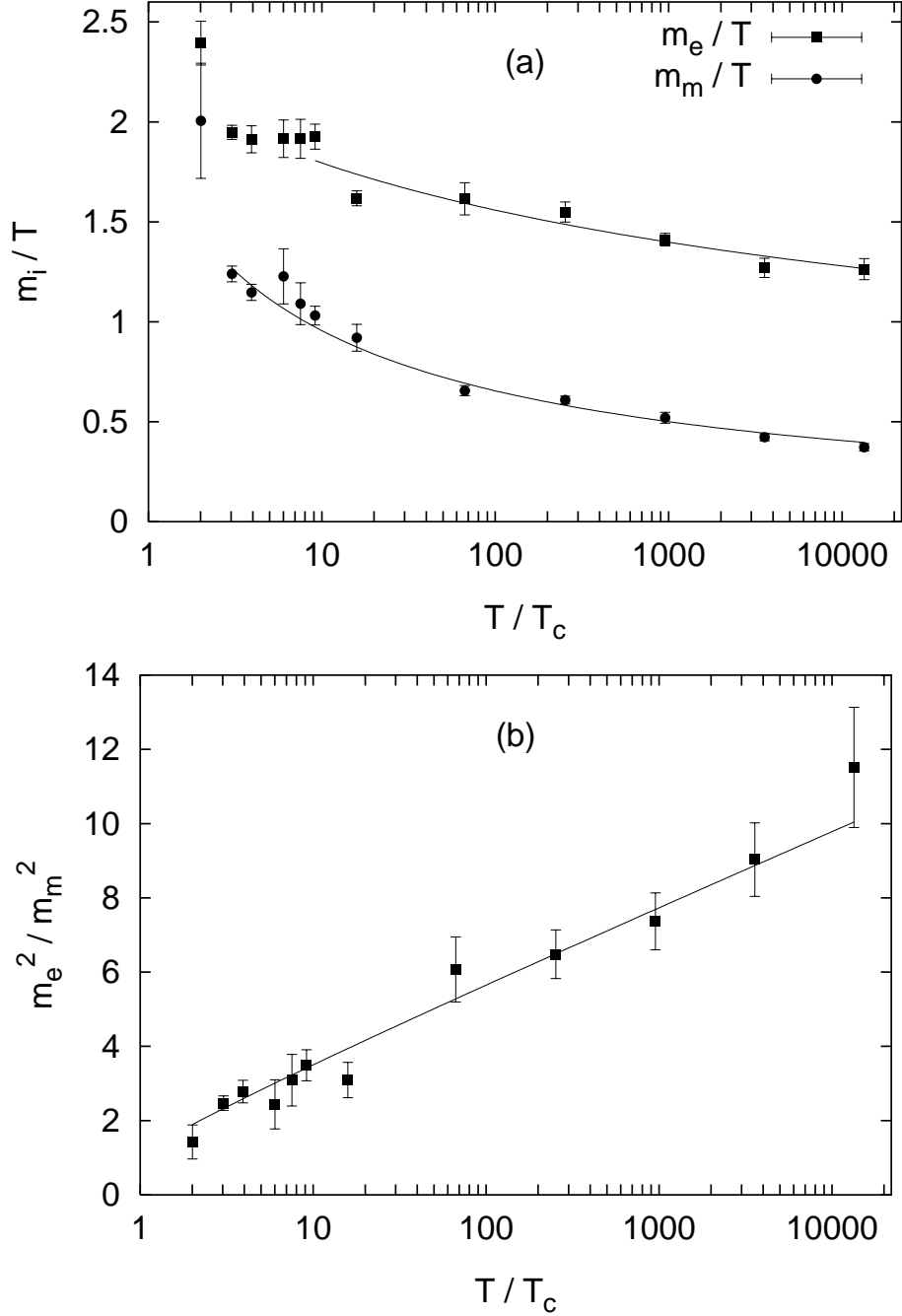


Figure 4: Electric and magnetic screening masses in units of the temperature (a) and squared ratio of the masses (b) vs. T/T_c . Data are obtained from simulations on a $32^2 \times 64 \times 8$ lattice using the Wilson action.

$T \geq 250 T_c$. A one parameter fit at fixed $T_c/\Lambda_{\overline{\text{MS}}} = 1.06$ gives $B_{\text{fit}} = 0.744(28)$ with $\chi^2/\text{dof} = 4.55$ (dotted line in Fig. 3).

Let us now return to the discussion of the magnetic mass. As noted above, the ratio m_e/m_m suggests a magnetic mass of the form $m_m(T) \sim g^2(T) T$. Therefore we fitted m_m with the ansatz

$$\frac{m_m(T)}{T} = D_{\text{fit}} g^2(T) \quad . \quad (4.7)$$

The two parameter fit of m_m for $T \geq 3 T_c$ results in $D_{\text{fit}} = 0.478(17)$ and $\Lambda_{\text{fit}}/\Lambda_{\overline{\text{MS}}} = 0.77(14)$ with $\chi^2/\text{dof} = 1.44$. This is in good agreement with our result obtained in [11] for $T < 20 T_c$. With a fixed Λ -parameter, $T_c/\Lambda_{\overline{\text{MS}}} = 1.06$, we obtain $D_{\text{fit}} = 0.456(6)$ and $\chi^2/\text{dof} = 1.53$. In Fig. 4a the two parameter fit is shown. The small deviation of the fitted curve from the measured data shows that the magnetic mass indeed is well described by the functional form $m_m(T) \sim g^2(T) T$.

The analysis of m_m/T and m_e/m_m is, of course, consistent with our most straightforward fit to the electric mass, $m_e(T) = \sqrt{1.69(2)} g(T) T$. In contrast to the fit based on ansatz (4.6) this fit describes the data well in the entire temperature range above T_c . This shows that the electric mass has a strong non perturbative character in the temperature interval we have investigated.

4.2 Numerical Results for Non-Zero Momenta

Let us briefly discuss the gluon correlation functions at non-zero momenta. As the numerical signal gets lost in statistical noise for high momenta (see (2.3) and (4.1)) we only could analyse the cases $k_1 = 1, 2$, i.e. $p_1 a = 2\pi/N_1, 4\pi/N_1$. Furthermore, we only obtained a reliable result in the electric sector. From Eq. (4.1) we have

$$\sinh^2 \frac{aE_e(p_1)}{2} = \sinh^2 \frac{am_e}{2} + \kappa \sin^2 \frac{ap_1}{2} \quad . \quad (4.8)$$

For m_e we use the result from the measurement at zero momentum. In the limit $T \rightarrow \infty$ one expects to find a free particle dispersion relation, i.e. $\kappa \rightarrow 1$. In Fig. 5 we have plotted κ vs. T/T_c . Obviously we do not have sufficient statistics to uncover

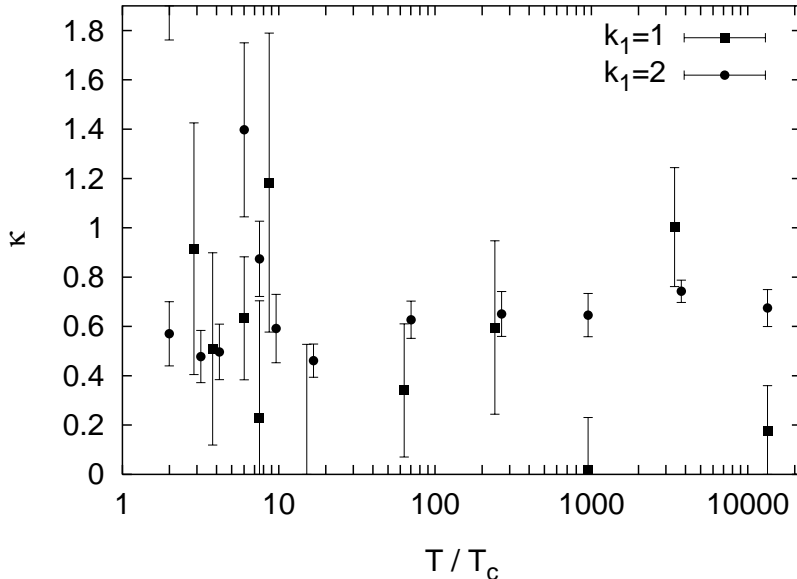


Figure 5: κ vs. T/T_c for $k_1 = 1, 2$. Some data points have been displaced horizontally for better viewing.

a temperature dependence of κ . Therefore we only quote a value averaged over the temperature interval $T \geq 9T_c$. We find $\kappa = 0.37(10)$ for $k_1 = 1$ and $\kappa = 0.65(3)$ for $k_1 = 2$. This suggest a quite significant modification of the free particle dispersion relation at low momenta.

5 Polyakov Loop Correlation Functions

It is well known that for temperatures above the critical temperature T_c , the confinement potential between a quark and an anti-quark is replaced by the color averaged potential [20], which, in lowest order perturbation theory, is of the form

$$V_{\text{av}}(R, T) \sim \frac{1}{TR^2} e^{-2m_e(T)R} \quad \text{for } T > T_c \quad . \quad (5.1)$$

Here m_e is the electric (or Debye) screening mass. As V_{av} decreases very fast, the numerical signal gets lost in statistical noise in the long distance regime. On the other hand, (5.1) is only valid at large distances. This situation is improved for the color singlet potential, which to leading order perturbation theory is controlled by

1-gluon exchange and therefore takes on the form

$$V_1(R, T) = -g^2 \frac{N_c^2 - 1}{8\pi N_c} \cdot \frac{e^{-m_e(T)R}}{R} \quad \text{for } T > T_c \quad . \quad (5.2)$$

The color singlet potential, however, is gauge dependent and one therefore again has to fix a gauge for its calculation. As mentioned earlier we have chosen the Landau gauge.

On the lattice one can extract both potentials by measuring Polyakov loop correlation functions [20],

$$e^{-V_{\text{av}}(R, T)/T} = \frac{\langle \text{Tr } L(\vec{R}) \text{Tr } L^\dagger(\vec{0}) \rangle}{\langle |L|^2 \rangle} \quad , \quad (5.3)$$

$$e^{-V_1(R, T)/T} = 2 \frac{\langle \text{Tr } (L(\vec{R}) L^\dagger(\vec{0})) \rangle}{\langle |L|^2 \rangle} \quad . \quad (5.4)$$

5.1 Improvement of the Singlet Potential

In this section we want to discuss briefly the improvement of rotational symmetry for the color singlet potential due to the use of an improved action. We have measured V_1/T both along an axis, labeled with $(1, 0, 0)$, and along three different off-axis directions, $(1, 1, 0)$, $(1, 1, 1)$, and $(2, 1, 0)$. To make the results from simulations with unimproved and improved action comparable, one has to choose couplings that both correspond to the same temperature. As an example, we use in the following $\beta_W = 3.219$ and $\beta_I = 2.652$. As listed in Tab. 1, both couplings correspond to $T \simeq 15.88 T_c$.

Motivated by Eq. (5.2) and taking into account the periodic boundary conditions, we have performed a correlated fit of the $(1, 0, 0)$ data in the interval^d $R \in [7, 12]$, using the fit function

$$V_{1,\text{fit}}(R, T) = A_{\text{fit}} \left(\frac{e^{-m_{\text{fit}}R}}{R} + \frac{e^{-m_{\text{fit}}(N_3-R)}}{N_3 - R} \right) \quad (5.5)$$

with $N_3 = 32$. The fit results for both actions are listed in Tab. 6. As one can see

^dSee App. A.

fit parameters	$\beta_W = 3.219$	$\beta_I = 2.652$
A_{fit}	-1.49(16)	-1.64(13)
m_{fit}	0.435(16)	0.416(11)
goodness	0.380	0.452
χ^2/dof	1.049	0.918
normalized χ^2 deviation from the (1, 0, 0) fit		
(1, 1, 0)	2.019	1.457
(1, 1, 1)	1.934	0.090
(2, 1, 0)	1.316	0.243

Table 6: Results from the fits of V_1/T at $\beta_W = 3.219$ and $\beta_I = 2.652$ ($T \simeq 15.88 T_c$).

from the upper part of the table, the fit itself is better for the improved data than for the Wilson data, i.e. the errors on the fit parameters are smaller, the goodness is higher and finally the squared error from the correlated fit (χ^2/dof) is smaller. The lower part of Tab. 6 shows the χ^2 deviation of the off-axis data points from the (1, 0, 0) fit curves. For this comparison we used data in the interval $7 \leq R \leq 12$ and divided by the number of points taken into consideration. For all measured off-axis directions these data show that the violation of rotational symmetry is lowered by going from the Wilson to the tree-level Symanzik improved action. This behavior becomes also clear from Fig. 6, which shows the potential V_1 (normalized by the fit function (5.5) with the parameters given in Tab. 6) vs. distance R .

5.2 The Electric Screening Mass from the Singlet Potential

We used on-axis point-to-point as well as plane-plane Polyakov loop correlation functions to extract the electric screening mass. In the former case, we used Eqs. (5.2) and (5.4) and performed a correlated fit of the numerical data, using (5.5) and the fit criterium described in App. A. We did this both for the measurement along the (1,0,0) axis and for the three different off-axis directions mentioned in Sec. 5.1.

In the second case, the expression for the Polyakov loop $L(\vec{R})$ in Eq. (5.4) is

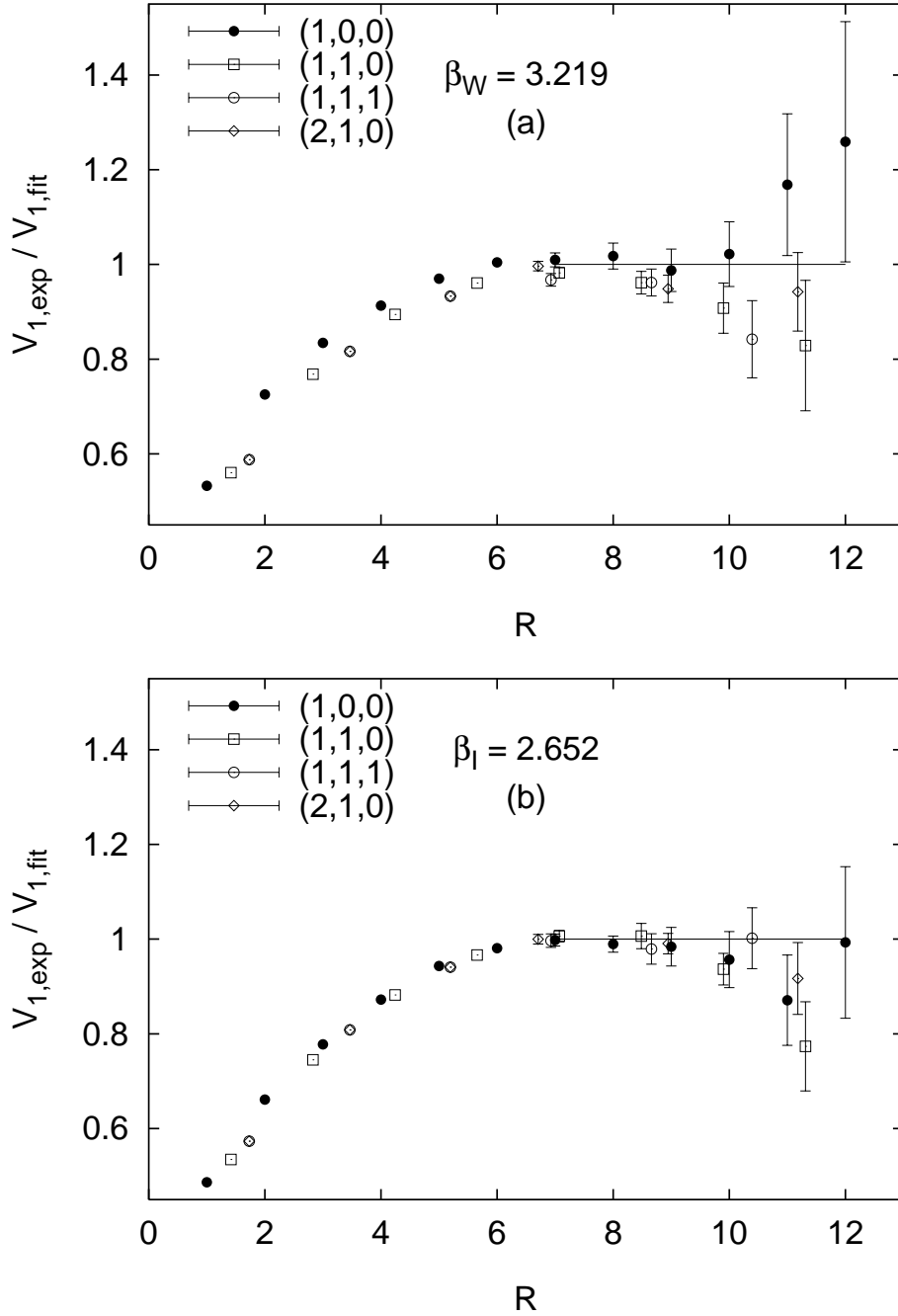


Figure 6: Singlet potential $V_1(R)$, normalized by the correlated fit of the $(1,0,0)$ -data in the interval $R \in [7, 12]$. The data have been calculated on a lattice of size $32^3 \times 4$ using the Wilson action at $\beta_W = 3.219$ (a) and the Symanzik action at $\beta_I = 2.652$ (b). Both couplings correspond to a temperature of $T \simeq 15.88 T_c$. The different symbols refer to the (x_1, x_2, x_3) -directions along which the measurements have been performed.

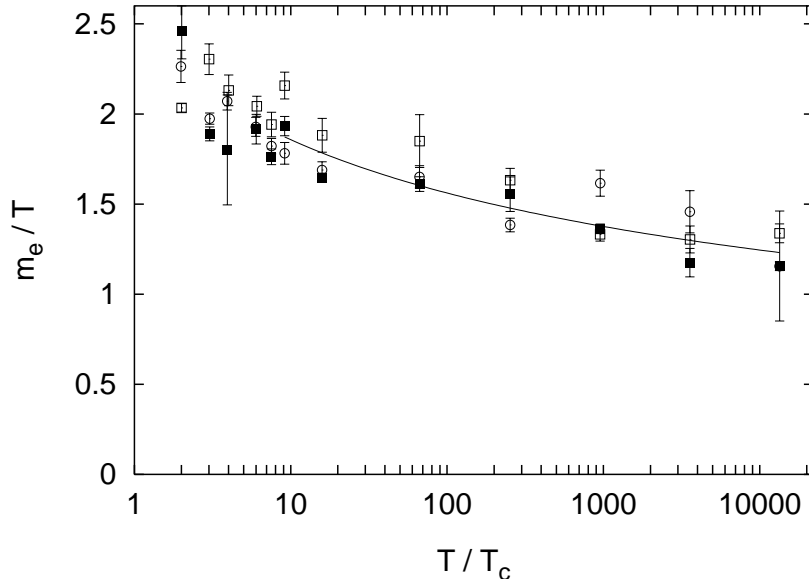


Figure 7: Electric screening masses, obtained from $V_{1,\text{sum}}$. The data points refer to the same lattice sizes and actions as in Fig. 3. The solid line is a one parameter fit for $T \geq 9 T_c$, using ansatz (4.4).

replaced by $L(x_3) \equiv \sum_{x_1, x_2} L(x_1, x_2, x_3)$. Then (5.4) and (5.2) transform into

$$e^{-V_{1,\text{sum}}(x_3, T)/T} = 2 \frac{\langle \text{Tr} (L(x_3) L^\dagger(0)) \rangle}{\langle |L| \rangle^2} \quad (5.6)$$

and

$$V_{1,\text{sum}}(x_3, T) \sim e^{-m_e(T)x_3} \quad \text{for } T > T_c \quad . \quad (5.7)$$

Whereas we have calculated V_1 on lattices of size $32^3 \times 4$ and $32^2 \times 64 \times 8$ and for both actions, we have calculated $V_{1,\text{sum}}$ only on the larger lattice, using the Wilson action. The results for the electric screening mass are listed in Tab. 7 and 8.

Similar to the electric mass extracted from gluon correlation functions, the results we have now obtained with different actions and on lattices of varying size again do not differ significantly. Therefore we have also here analysed all three datasets together. The screening masses, extracted from $V_{1,\text{sum}}$, are shown in Fig. 7.

As expected from Sec. 4, m_e/T , extracted now from Polyakov loop correlation functions, also depends only weakly on the temperature for temperatures less than

Wilson action, $32^3 \times 4$ lattice					
β_W	$m_e(T)/T$, extracted from				
	$V_{1,\text{sum}}$	$V_{1,(1,0,0)}$	$V_{1,(1,1,0)}$	$V_{1,(1,1,1)}$	$V_{1,(2,1,0)}$
2.512	2.03(2)	2.28(9)	2.22(4)	2.13(4)	2.38(11)
2.643	2.30(9)	2.15(6)	2.12(5)	2.07(4)	2.25(9)
2.74	2.13(9)	2.09(5)	2.04(5)	2.04(4)	2.14(7)
2.88	2.04(6)	1.95(6)	1.91(3)	1.93(2)	1.96(7)
2.955	1.94(7)	2.11(8)	1.97(5)	1.94(6)	2.06(5)
3.023	2.16(7)	1.84(5)	2.01(4)	1.96(9)	1.98(6)
3.219	1.88(9)	1.74(6)	1.80(4)	1.75(5)	1.83(4)
3.743	1.85(15)	1.50(2)	1.50(1)	1.43(2)	1.61(3)
4.24	1.63(7)	1.55(9)	1.53(7)	1.45(3)	1.44(2)
4.738	1.33(4)	1.75(10)	1.32(5)	1.32(3)	1.29(2)
5.238	1.30(7)	1.29(4)	1.25(4)	1.20(2)	1.19(2)
5.737	1.34(5)	1.29(3)	1.24(4)	1.17(1)	1.15(2)

Symanzik action, $32^3 \times 4$ lattice					
β_I	$m_e(T)/T$, extracted from				
	$V_{1,\text{sum}}$	$V_{1,(1,0,0)}$	$V_{1,(1,1,0)}$	$V_{1,(1,1,1)}$	$V_{1,(2,1,0)}$
1.92	2.26(9)	2.04(4)	2.16(5)	2.12(5)	2.06(2)
2.063	1.97(3)	1.98(3)	2.01(3)	2.03(4)	2.12(7)
2.152	2.07(5)	2.16(8)	2.02(7)	2.04(4)	2.01(6)
2.30	1.93(5)	1.83(2)	1.79(3)	1.70(3)	1.84(4)
2.382	1.82(4)	1.83(3)	1.72(3)	1.70(2)	1.90(5)
2.452	1.78(6)	2.14(12)	1.98(14)	1.76(7)	1.79(5)
2.652	1.69(5)	1.66(4)	1.57(2)	1.54(2)	1.67(3)
3.183	1.65(6)	1.58(6)	1.62(5)	1.51(3)	1.48(2)
3.684	1.38(4)	1.71(12)	1.42(3)	1.36(3)	1.33(2)
4.185	1.62(7)	1.66(15)	1.34(3)	1.19(2)	1.21(66)
4.685	1.46(12)	1.22(3)	1.19(3)	1.10(2)	1.09(1)
5.186	1.16(2)	1.22(5)	1.14(3)	1.05(2)	1.03(1)

Table 7: Electric screening masses from Polyakov loop correlation functions.

Wilson action, $32^2 \times 64 \times 8$ lattice					
β_W	$m_e(T)/T$	β_W	$m_e(T)/T$	β_W	$m_e(T)/T$
2.74	2.46(16)	3.20	1.76(4)	4.50	1.55(10)
2.88	1.89(4)	3.27	1.93(5)	5.00	1.36(3)
2.97	1.80(31)	3.47	1.65(3)	5.50	1.18(8)
3.12	1.92(8)	4.00	1.61(4)	6.00	1.16(31)

Table 8: Electric screening masses from $V_{1,\text{sum}}$.

about $9T_c$. For example, fitting $V_{1,\text{sum}}$ in this temperature range with a constant, we obtain $m_e(T)/T = 2.010(13)$.

According to Sec. 4 we performed, for temperatures $T \geq 9T_c$, one parameter fits (i.e. $\Lambda_{\text{fit}}/\Lambda_{\overline{\text{MS}}} = 1$), using the ansatz (4.4). The results from the lattice of size $32^3 \times 4$ are summarized in Tab. 9. On the $32^2 \times 64 \times 8$ we obtain from $V_{1,\text{sum}}$ a fit

Wilson action, $32^3 \times 4$ lattice					
	Fits of $(m_e(T)/T)^2$, extracted from				
	$V_{1,\text{sum}}$	$V_{1,(1,0,0)}$	$V_{1,(1,1,0)}$	$V_{1,(1,1,1)}$	$V_{1,(2,1,0)}$
A_{fit}	1.97(6)	1.70(3)	1.60(2)	1.53(2)	1.61(2)
χ^2/dof	2.49	10.6	6.64	7.29	4.18

Symanzik action, $32^3 \times 4$ lattice					
	Fits of $(m_e(T)/T)^2$, extracted from				
	$V_{1,\text{sum}}$	$V_{1,(1,0,0)}$	$V_{1,(1,1,0)}$	$V_{1,(1,1,1)}$	$V_{1,(2,1,0)}$
A_{fit}	1.67(4)	1.46(2)	1.46(2)	1.35(2)	1.36(2)
χ^2/dof	7.10	15.0	10.8	4.51	5.72

Table 9: Fit results of $(m_e(T)/T)^2$, extracted from Polyakov loop correlation functions, using the fit ansatz (4.4).

value $A_{\text{fit}} = 1.72(4)$ with $\chi^2/\text{dof} = 4.60$.

In general we find that the results extracted from $V_{1,\text{sum}}$ are in good agreement with the zero momentum results from the gluon correlation functions. To make this clear also quantitatively we have analyzed all three datasets for $V_{1,\text{sum}}$ together, as

in the case of the gluon correlation functions. The one parameter fit for $T \geq 9T_c$ yields $A_{\text{fit}} = 1.71(2)$ with $\chi^2/\text{dof} = 5.80$. This can be compared with the result from Tab. 5, $A_{\text{fit}} = 1.69(2)$ with $\chi^2/\text{dof} = 4.51$. We therefore conclude that the electric screening mass is well described by $m_e(T) = \sqrt{1.70(2)} g(T) T$ in the temperature range $T \leq 14000 T_c$.

6 Summary and Conclusions

We have studied Polyakov loop and gluon correlation functions in the high temperature deconfined phase of SU(2) lattice gauge theory in a wide range of temperatures, using both the standard Wilson action and a tree-level Symanzik improved action. We have calculated chromo-electric and -magnetic screening masses and have determined their dependence on the temperature.

The temperature dependence found for the magnetic mass is in accordance with the expected $g^2(T)$ -dependence. We find $m_m(T) = 0.456(6) g^2(T) T$. The behavior of the electric mass shows, however, that this does not at all mean that the screening masses can be described according to perturbative expectations. Although the temperature dependence of m_e is consistent with a logarithmic dependence, $m_e \sim gT$, our data do not agree with lowest order perturbation theory. Only little improvement is achieved by using next-to-leading order results from resummed PT. From an analysis of the gluon propagator as well as the color singlet potential we find $m_e(T) = \sqrt{1.70(2)} g(T) T$. This result shows that the screening mechanism is highly non-perturbative even for temperatures as large as $14000 T_c$. This observation is in accordance with studies of screening in dimensionally reduced 3d-QCD [8, 9].

Our simulation of the gluon correlation functions at finite momenta still suffer from insufficient statistics. We find a modification of the energy momentum dispersion relation of a free particle, but we are not yet able to quantify its temperature dependence.

The improvement of the action does not show, within statistical errors, any significant modification of the behavior of the screening masses, although we can show that the violation of the rotational symmetry of the singlet potential, which

also was used to extract m_e , is weakened.

Acknowledgements: The work of FK has been supported through the Deutsche Forschungsgemeinschaft under grant Pe 340/3-3 and the work of UMH and JR, in part, by the US DOE under grants DE-FG05-85ER25000 and DE-FG05-96ER40979. JR acknowledges a graduate scholarship of North-Rhine-Westfalia and support by the DAAD.

Appendix

A Determination of Screening Masses from Correlation Functions

To shorten the discussion, we assume in this section the case of vanishing momentum. Taking periodic boundary conditions into account, it follows from Eqs. (2.3) and (4.1) that the electric and magnetic screening masses are related to the long-distance behavior of the gauge field correlation functions $G_e(x_3) \equiv G_e(p_\perp = 0, x_3)$ and $G_m(x_3) \equiv G_m(p_\perp = 0, x_3)$ via

$$G_i(x_3) \sim \cosh \left\{ m_i \left(x_3 - \frac{N_3}{2} \right) \right\} \quad \text{for } x_3 \gg 1 \text{ and } i = e, m. \quad (\text{A.1})$$

As there is generally no unique rule how to select the interval in which $G_e(x_3)$ and $G_m(x_3)$ should be fitted, we have constructed a criterium how to find a suitable fit interval for a given set of numerical data.

A fit is in general characterized by several properties, namely χ^2 , goodness (Q), degrees of freedom (ϱ) and relative errors of the fit parameters. As χ^2 enters directly into the calculation of Q , it is sufficient to consider only the last three quantities. It is desirable to find a fit with large Q , large ϱ and small relative error on the fit parameter we are interested in, i.e. on m_i/T . As we want to weigh these three quantities, we are looking for a fit interval with

$$Q^\alpha \cdot \varrho^\beta \cdot \left(\frac{\Delta m_i}{m_i} \right)^{-\gamma} \rightarrow \max \quad . \quad (\text{A.2})$$

We have chosen the coefficients to be $\alpha = 9$, $\beta = 1$ and $\gamma = 3$. As we put the largest weight on Q , it sometimes happens that only a very small fit interval is selected by this condition. To avoid this problem, we add the extra condition $\varrho \geq 3$. For a two parameter fit this is equivalent to demand that the fit interval should contain at least 5 points.

Finally we require that the fit only considers points $G_e(x_3)$ or $G_m(x_3)$ with errors less than 50 % of their value. This is to reject points that are dominated by statistical noise.

To see how our fit criterium works we show in Fig. 8 $G_e(x_3)$ vs. x_3 for one arbitrary

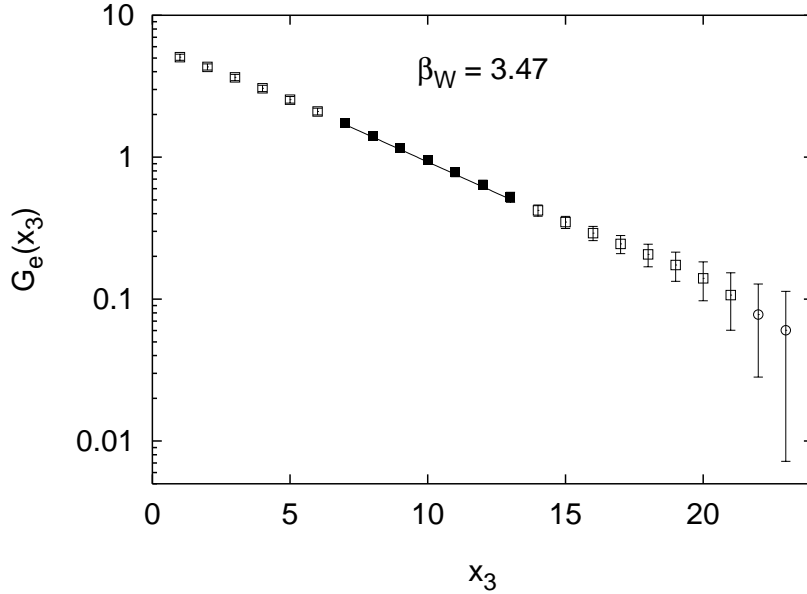


Figure 8: The electric correlation function $G_e(x_3)$ as a function of x_3 calculated on a lattice of size $32^2 \times 64 \times 8$ using the Wilson action at $\beta_W = 3.47$. The squares show points with an error less than 50% of the value, whereas the circles describe points with a bigger error. The filled points represent the fit interval, found by our fit criterium. The solid line is the correlated fit.

coupling, $\beta_W = 3.47$. The solid line is the correlated fit, found automatically by the fit criterium. To demonstrate the quality of the fit criterium, we have also studied local screening masses $m_i(x_3)$. They are defined by the relation ($a = 1$)

$$\frac{G_i(x_3)}{G_i(x_3 + 1)} = \frac{\cosh\left(m_i(x_3)\left(x_3 - \frac{N_3}{2}\right)\right)}{\cosh\left(m_i(x_3)\left(x_3 + 1 - \frac{N_3}{2}\right)\right)}, \quad i = e, m \quad . \quad (\text{A.3})$$

If x_3 becomes large enough, $m_i(x_3)$ must reach a plateau. On the other hand, if x_3 becomes too large, the local masses have big statistical errors and do not carry valuable information.

In Fig. 9 we show the local electric screening masses in units of the temperature,

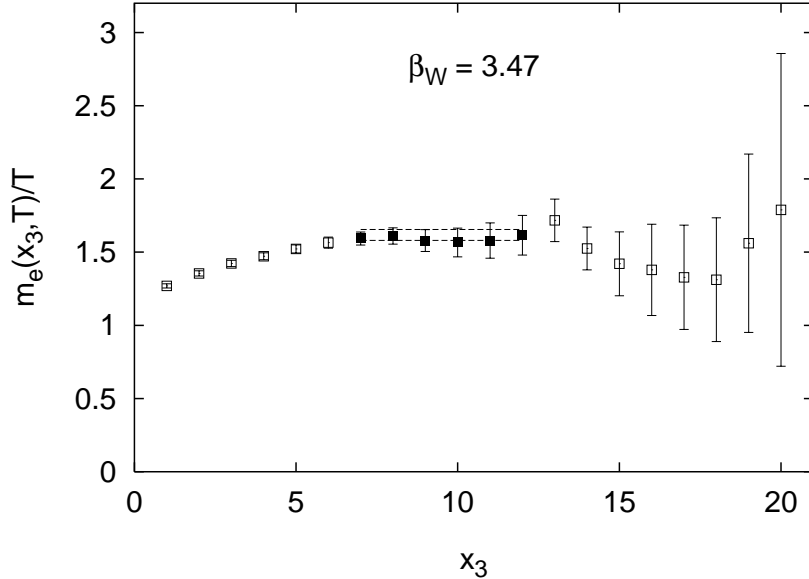


Figure 9: Local electric screening masses, extracted from the electric correlation function $G_e(x_3)$ shown in Fig. 8. The horizontal lines are the lower and upper bounds for $m_e(T)/T$, given by the correlated fit shown in Fig. 8.

$m_e(x_3, T)/T$, extracted from $G_e(x_3)$ shown in Fig. 8. The horizontal lines are the lower and upper bounds for $m_e(T)/T$, given by the correlated fit shown in Fig. 8. Obviously, the fit criterium works fine and finds a reliable fit interval.

References

- [1] A.D. Linde, Phys. Lett. **B96** (1980) 289.
- [2] A.K. Rebhan, Phys. Rev. **D48** (1993) R3967.
- [3] A.K. Rebhan, Nucl. Phys. **B430** (1994) 319.
- [4] J.-P. Blaizot and E. Iancu, Nucl. Phys. **B459** (1996) 559.

- [5] R. Kobes, G. Kunstatter, A. Rebhan, Phys. Rev. Lett. **64** (1990) 2992.
- [6] R. Kobes, G. Kunstatter, A. Rebhan, Nucl. Phys. **B355** (1991) 1.
- [7] P. Arnold and L. G. Yaffe, Phys. Rev. **D52** (1995) 7208.
- [8] K. Kajantie, M. Laine, K. Rummukainen and M. Shaposhnikov, hep-ph/9704416, April 1997.
- [9] K. Kajantie, M. Laine, J. Peisa, A. Rajantie, K. Rummukainen, M. Shaposhnikov, hep-lat/9709024, September 1997.
- [10] F. Karsch, T. Neuhaus, A. Patkós and J. Rank, Nucl. Phys. **B474** (1996) 217.
- [11] U.M. Heller, F. Karsch and J. Rank, Phys. Lett. **B355** (1995) 511.
- [12] H.Th. Elze, K. Kajantie and J. Kapusta, Nucl. Phys. **B304** (1988) 832.
- [13] J. Engels, F. Karsch and H. Satz, Nucl. Phys. **B205** (1982) 239.
- [14] B. Beinlich, F. Karsch and E. Laermann, Nucl. Phys. **B462** (1996) 415.
- [15] J. Engels, F. Karsch and K. Redlich, Nucl. Phys. **B435** (1995) 295.
- [16] J. Fingberg, U.M. Heller and F. Karsch, Nucl. Phys. **B392** (1993) 493.
- [17] G. Cella, G. Curci, R. Tripicciono and A. Vicere, Phys. Rev. **D49** (1994) 511.
- [18] W. Bernreuther and W. Wetzel, Phys. Lett. **B132** (1983) 382; P. Weisz and R. Wohlert, Nucl. Phys. **B236** (1984) 397; **B247** (1984) 544(E).
- [19] R. Dashen and D.J. Gross, Phys. Rev. **D23** (1981) 2340.
- [20] L.D. McLerran and B. Svetitsky, Phys. Rev. **D24** (1981) 450.